ARTICLE   OPEN

Normal-state charge transport in YBa$_2$Cu$_3$O$_{6.67}$ under uniaxial stress

S. Nakata [1], P. Yang [2], M. E. Barber [2], K. Ishida [2], H.-H. Kim[1], T. Loew[1], M. Le Tacon [3], A. P. Mackenzie [2,4], M. Minola [1], C. W. Hicks [2] and B. Keimer [1]✉

To provide a foundation for theoretical models of high-temperature superconductivity, experimental research has sought to establish correspondences between macroscopic transport coefficients on the one hand, and atomic-scale correlation functions measured by spectroscopic and scattering probes on the other hand. This research avenue has been confounded by the gradual onset of electronic ordering phenomena and of the corresponding transport anomalies. We report measurements of the uniaxial-stress dependence of the normal-state resistivity and Hall coefficient of the underdoped high-temperature superconductor YBa$_2$Cu$_3$O$_{6.67}$. We observe a remarkable correspondence between the differential stress responses of the transport coefficients and resonant X-ray diffraction features indicative of charge ordering, which parallels the phenomenology of classical charge-density-wave compounds. However, our observations imply that static charge order is not responsible for a sign reversal of the Hall coefficient, and suggest that the interplay with liquid-like, dynamical charge correlations is essential for the prominent transport anomalies in the underdoped cuprates.

INTRODUCTION

Nuclear magnetic resonance (NMR) and X-ray scattering experiments have recently identified charge order as a universal feature of the layered cuprates, and as the leading competitor of high-temperature superconductivity at moderate doping levels[1–3]. However, the fact that there is no sharply defined transition or onset temperature apparent in the thermal evolution of either direct measures of the charge order, or of any transport properties, makes it difficult to establish a correspondence between the two sets of observables. Recently, external control parameters have opened up fresh perspectives on this key issue. Specifically, the application of external magnetic fields of order 100 T has revealed a wealth of new information about quantum transport phenomena in the cuprates[4–9], but the application of complementary spectroscopic and scattering probes under these extreme conditions remains a major challenge[10–13]. Hydrostatic pressure is another continuously tunable parameter, but corresponding studies have so far yielded seemingly contradictory results. Whereas X-ray scattering experiments indicate a complete suppression of charge order under modest pressure[14], purported transport and NMR data signatures of charge order are only weakly pressure dependent[15–17]. However, the measurements were carried out on different samples and partly in high magnetic fields, which are known to enhance the charge ordering. In conjunction with the strong dependence of the doping level on hydrostatic pressure, these difficulties have so far precluded firm conclusions.

Recent experimental advances have enabled the application of highly homogeneous uniaxial stress to complex quantum materials, thereby opening up additional perspectives for in situ experiments with a continuously tunable parameter[18–28]. The application of stress in X-ray scattering experiments has already uncovered substantial modifications of the charge-ordered state

of the cuprates[29,30]. However, transport measurements under high stress are difficult because even minor stress-induced cracks can disrupt the current flow. Despite the recent methodological progress, only few complementary studies on the stress response of transport coefficients in cuprates have been reported[31]. We report measurements of the stress dependence of the normal-state resistivity and Hall coefficient of twin-free single crystals of the underdoped high-T_c superconductor YBa$_2$Cu$_3$O$_{6+x}$ (YBCO$_{6+x}$), which is particularly suitable for such experiments because of its low degree of lattice disorder (Fig. 1a). We chose the doping level of ~0.12 holes per copper ion ($x = 0.67$) where charge ordering is most pronounced[32]. A substantial stress-induced enhancement of the charge order was recently observed on crystals identical to those investigated here, using a nearly identical experimental setup[29,30]. We find remarkable parallels in the stress responses of the transport coefficients and the diffraction signal from static charge-ordering, especially with regard to their temperature evolution and in-plane anisotropy. This correspondence allows us to conclude that the condensation of collective charge fluctuations reduces the resistivity, similar to classical charge-density-wave (CDW) materials with quasi-two-dimensional (2D) electron systems, where this effect has been attributed to a loss of inelastic scattering channels in the CDW state[33–35]. However, we also conclude that the impact of static charge order is too weak to explain the most prominent transport anomalies, including the well-known sign reversal of the Hall coefficient as a function of temperature[6]. We argue that in YBCO$_{6.67}$, liquid-like collective fluctuations of the electron system take on the role of static order in the classical CDW compounds, and we point out the need to develop a theoretical framework to describe the underlying mechanisms[36]. Our results illustrate the potential of uniaxial-pressure experiments with multiple complementary probes to elucidate the correspondence between atomic-scale electronic

[1]Max Planck Institute for Solid State Research, Heisenbergstraße 1, D-70569 Stuttgart, Germany. [2]Max Planck Institute for Chemical Physics of Solids, Nöthnitzer Straße 40, 01187 Dresden, Germany. [3]Institute for Quantum Materials and Technologies, Karlsruhe Institute of Technology, D-76344 Eggenstein-Leopoldshafen, Germany. [4]Scottish Universities Physics Alliance, School of Physics and Astronomy, University of St Andrews, St Andrews KY16 9SS, UK. ✉email: b.keimer@fkf.mpg.de
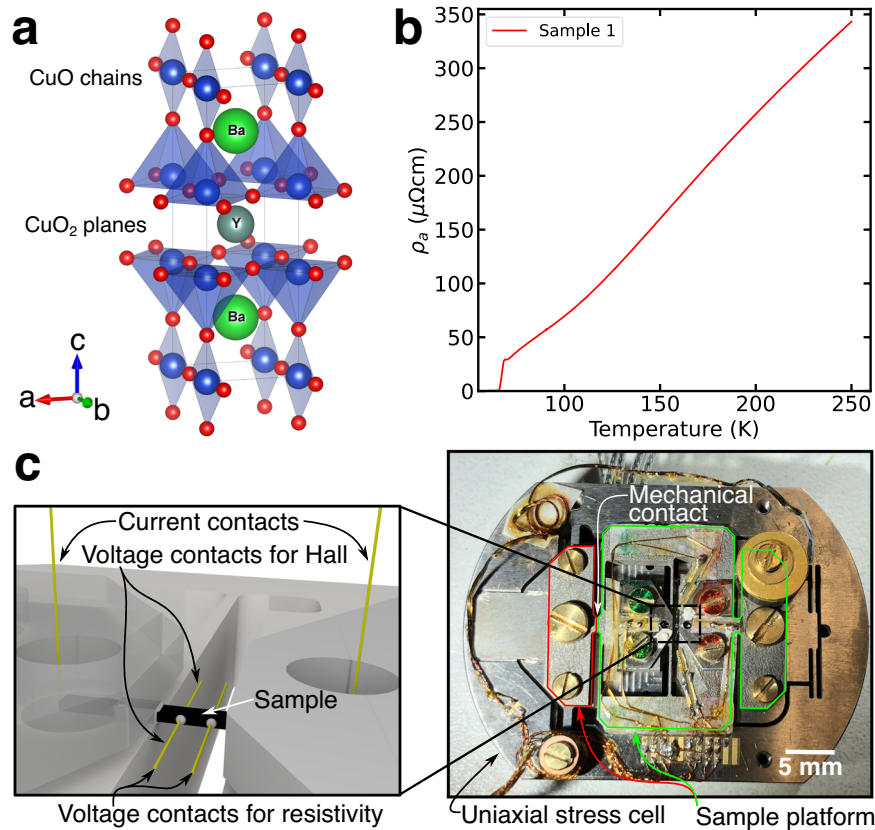
Fig. 1 Measurement setup. a Unit cell of YBa$_2$Cu$_3$O$_7$[61]. Blue and red spheres represent Cu and O atoms, respectively. **b** Resistivity ρ_a in the absence of stress. **c** Schematic of the sample mounted on the uniaxial stress cell seen from the side (left). Top view of the stress cell (right). Sample platforms incorporated a mechanical contact are marked by red and green (Supplementary Note 2).

correlations and macroscopic transport phenomena in quantum materials.

RESULTS AND DISCUSSION
Resistivity measurements
The single crystals of YBCO$_{6.67}$ were grown using the flux method[37]. The oxygen content was controlled by annealing the samples at 555 °C in a mixture of 5% O$_2$ and 95% Ar for one week[38]. The samples were then detwinned mechanically[39]. The superconducting $T_c = 65$ K was determined by magnetometry (Supplementary Note 1), and the hole doping $p \sim 0.12$ was estimated from the c-axis lattice constant measured by X-ray diffraction at room temperature[40]. To maximize the homogeneity of the uniaxial stress, the samples were cut into rectangular blocks with typical dimensions ~ 2.5 mm $\times 0.2$ mm $\times 0.1$ mm[41], and the stress was applied along the long axis. We studied two samples with long axes along the a-direction of the CuO$_2$ layers (samples 1 and 3), and one sample (sample 2) with long axis along b, the direction of the CuO chains in the crystal structure (Fig. 1a). The resistivity ρ and Hall coefficient R_H were measured in a standard four-probe configuration (see "Methods"). The temperature-dependent resistivity at ambient pressure measured in this way is consistent with prior reports, including signatures of pseudogap formation at temperatures around 200 K, well above the onset of charge order (Fig. 1b)[42].

We pressurized the samples using a piezoelectric-based apparatus, illustrated in Fig. 1c, that incorporated sensors of both the force and displacement applied to the sample[43–45]. From the applied force, the stress in the sample can be accurately determined, independently of the deformation of the epoxy that

holds the sample. Therefore, in the present study, we discuss the pressure effect in terms of stress (denoted as σ_{xx} and σ_{yy} for a and b-axis pressure, with negative sign for compressive stress). Additionally, in stress-sweep measurements, the samples were mounted onto platforms incorporating a mechanical contact that opens when the force falls to zero. This feature prevents the application of tensile stress, but allows accurate in situ calibration of the zero-force position (Supplementary Note 2). Note that the strain levels covered in the present study are below the onset strain of the three-dimensional (3D) charge order observed in recent X-ray scattering experiments[29,30]. Our study is thus limited to the possible influence of strain-enhanced 2D charge order on the transport coefficients.

Figure 2 shows the normalized electrical resistance, $\Delta R/R$, as a function of stress along the principal in-plane directions a and b for different temperatures. (Note that we plot the measured resistance rather than the resistivity because of the stress-dependent sample geometry, as discussed below.) Throughout the entire temperature range, $\Delta R/R$ shows a linear dependence on stress along both directions, but the amplitude and sign of the stress response evolve strongly with temperature. Figure 3a summarizes the temperature dependence of the stress response deduced from linear fits of the $\Delta R/R$-versus-σ curves in Fig. 2. Since σ is negative throughout our study, we plot the stress derivative $-\mathrm{d}(\Delta R/R)/\mathrm{d}\sigma$, which is positive (negative) if the resistivity increases (decreases) with increasing compression. Temperature sweep experiments of $\Delta R/R$ for fixed a-axis compression yield consistent results (sample 3 in Fig. 3a). The temperature dependence of $-\mathrm{d}(\Delta R/R)/\mathrm{d}\sigma$ is qualitatively similar for a- and b-axis compression, with a maximum at $T \sim 150$ K followed by a zero-crossing around 100 K. We, therefore, attribute this behavior to electrons in the CuO$_2$ layers, rather than the CuO chains. However, we note that
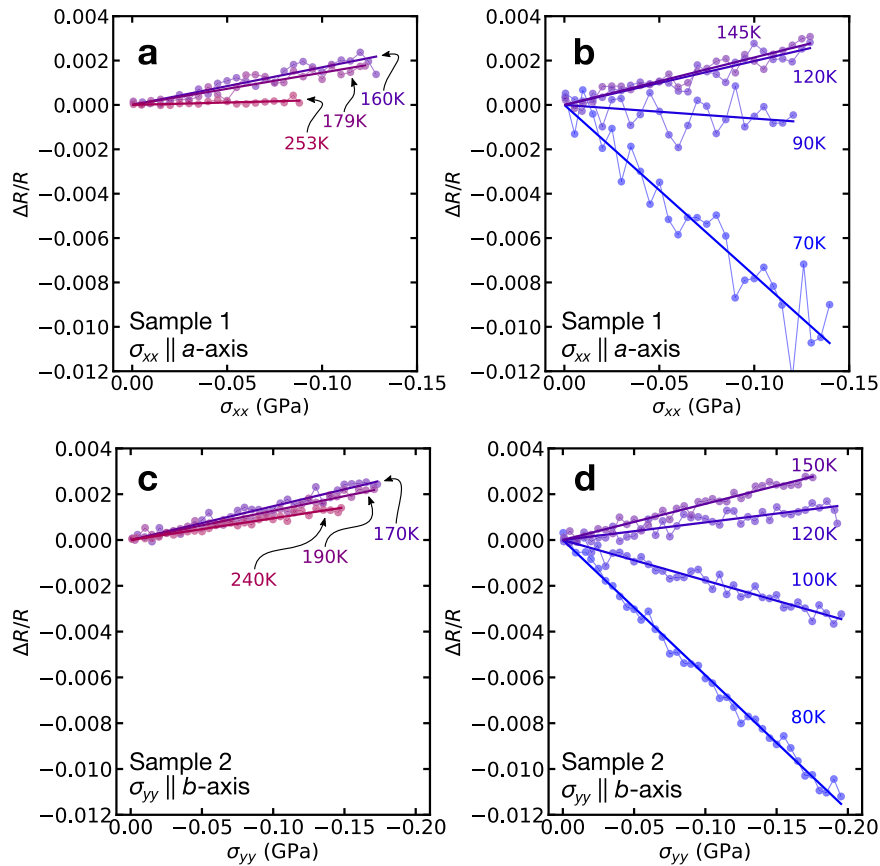
Fig. 2 Stress sweep measurements of the normalized electrical resistance. a Change of resistance $\Delta R/R$ vs. uniaxial stress σ_{xx} for different temperatures above $T = 150$ K. The resistance R was measured and σ_{xx} was applied along the a-axis. Solid lines are the results of linear fits. **b** Same as (**a**), with $T \leq 150$ K. **c, d** Same as (**a, b**) with R and σ_{yy} parallel to the b-axis.

both the onset of the downturn and the zero-crossing are observed at higher temperature for stress along b, and that the amplitude of $-d(\Delta R/R)/d\sigma_{yy}$ at low T substantially exceeds the one of $-d(\Delta R/R)/d\sigma_{xx}$ (Fig. 3a).

In interpreting these results, we first consider the impact of stress on the sample geometry, which affects the measured resistance $R = \rho l/A$ via the length l and cross-sectional area A of the sample. Specifically,

$$\frac{d(\Delta R/R)}{d\varepsilon_{xx}} = \frac{d(\Delta \rho/\rho)}{d\varepsilon_{xx}} + (1 + v_{xy} + v_{xz}),\qquad(1)$$

where ρ is the resistivity, $\varepsilon_{xx} = \sigma_{xx}/E_x$ is the strain (with the Young's modulus $E_x \sim 160$ GPa), and $(v_{xy}, v_{xz}) \sim (0.44, 0.16)$ are the Poisson's ratios[46]. As $1 + v_{xy} + v_{xz}$ is positive, the geometric contribution to $-d(\Delta R/R)/d\sigma = -(1 + v_{xy} + v_{xz})/E_x \sim -0.01$ GPa^{-1}, is negative and nearly temperature-independent at all temperatures, contrary to the measured pressure response (Fig. 3a and Supplementary Note 3).

Likewise, contributions to the intrinsic $\Delta\rho/\rho$ arising from the stress dependence of the electronic hopping parameters are expected to decrease monotonically with compression (see Supplementary Note 4 for corresponding tight-binding calculations). The strong, non-monotonic temperature dependence of the stress response at lower temperatures indicates many-body correlations of the electron system.

In view of the recent observation of strongly T-dependent incommensurate charge order by X-ray diffraction on samples of identical composition[47], we compare our transport data to the amplitude of the diffraction signal arising from 2D charge order, which is displayed in Fig. 3b. We note that the onset of the downturn in $-d(\Delta R/R)/d\sigma$ (Fig. 3a) occurs just below the onset

temperature of the charge order signal around $T_{CO} \sim 150$–160 K. The in-plane anisotropies of the stress response of both quantities also exhibit striking similarities. Specifically, stress along both principal in-plane axes enhances the charge-ordering signal with an amplitude that is larger along b than along a (Fig. 3b)[30], mirroring the amplitude and anisotropy of the stress response of the resistivity (Fig. 3a). These parallels suggest that the electrical resistivity is reduced by the onset of charge order. A similar effect has been observed in classical CDW compounds with 2D electron systems, where the CDW gap partially reconstructs the Fermi surface such that the impact of the reduced carrier density on the resistivity is over-compensated by the reduced scattering probability of the residual carriers[34,35].

Hall effect measurements

In light of these considerations, we now discuss measurements of the Hall coefficient, which are displayed in Fig. 4. In agreement with prior work in the absence of pressure, the Hall coefficient, R_H, is positive at high temperatures and exhibits a maximum on cooling below $T \sim 150$ K, followed by a zero-crossing at $T_0 \sim 70$ K[5,48]. Based in part on quantum oscillation measurements in high magnetic fields, these phenomena have been ascribed to the formation of electron pockets via a Fermi surface reconstruction possibly induced by charge ordering, among other factors such as anisotropies of the Fermi surface and the scattering rate[4,8,9]. In qualitative agreement with this scenario, the application of stress amplifies the downturn of R_H upon cooling below ~130 K (Fig. 4c), consistent with the stress-induced enhancement of the charge ordering amplitude inferred from X-ray diffraction[30]. The effect is again larger for stress along b than along a (Fig. 4c), mirroring the
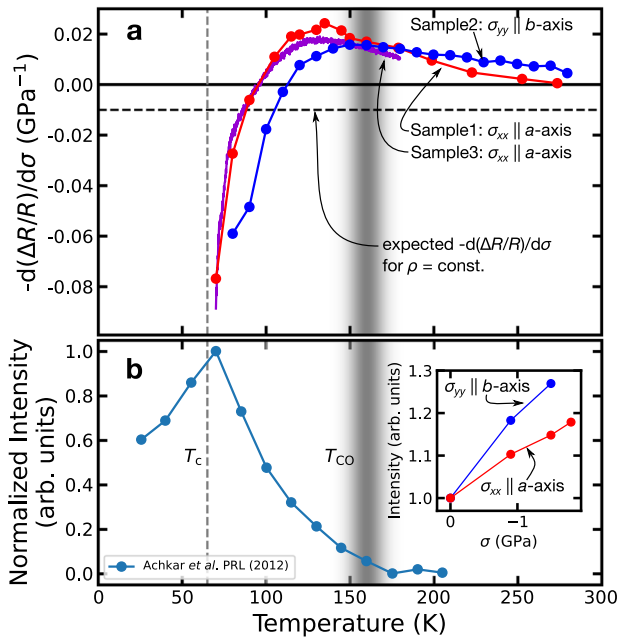
Fig. 3 Comparison of transport and diffraction signatures of charge order. a Stress response of the electrical resistance $-\mathrm{d}(\Delta R/R)/\mathrm{d}\sigma$ vs. temperature deduced from Fig. 2 (samples 1 and 2). Temperature sweep measurements at fixed stress are shown for an additional sample (sample 3). Here, the magnitude of $\Delta R/R$ was scaled by -1 GPa to convert the result to $-\mathrm{d}(\Delta R/R)/\mathrm{d}\sigma$. The horizontal dashed line marks the geometric contribution to $-\mathrm{d}(\Delta R/R)/\mathrm{d}\sigma$ for $\rho = $ constant (Supplementary Note 3). **b** Temperature dependence of the normalized intensity of the Bragg reflections characteristic of static charge-ordering measured by resonant X-ray scattering, reproduced from ref. [47]. The vertical dashed line and shaded area mark the superconducting transition temperature T_c and the onset of static charge order T_{CO}, respectively. Inset: Uniaxial stress dependence of the integrated peak intensity of both charge order domains with modulation propagating along the a- and b-directions, normalized to zero stress and summed together, extracted from the corresponding Bragg reflections[30] (Supplementary Note 5).

in-plane anisotropies of the longitudinal resistivity (Fig. 3a) and charge-ordering amplitude (Fig. 3b). On a qualitative level, our data thus provide additional implications of a Fermi-surface reconstruction induced by the experimentally observed charge correlations.

However, we note a large quantitative disparity in the stress responses of the charge ordering amplitude and the transport coefficients. In particular, the intensity of the X-ray reflections increases by ~100% for a-axis compression by 1 GPa[30], whereas only a small modification of R_H and a ~1 K shift of T_0 are observed under the same conditions (Fig. 4d). A related discrepancy was noted for hydrostatic pressure[15,16], which appears to affect the manifestations of charge order in scattering experiments much more strongly than the corresponding transport features[14]. In the latter case, however, the association is complicated by the influence of hydrostatic pressure on the doping level, which varies strongly as a function of doping and may obscure the comparison of data on different samples[17]. Moreover, some of the transport experiments were conducted in high magnetic fields, which also affect the amplitude of the charge order. Uniaxial stress, on the other hand, does not affect the doping level. This is evidenced by the observation that a stress-induced suppression of charge ordering has not been observed—neither in YBCO$_{6.67}$,[29,30] which is at the top of the charge-ordering 'dome' in the phase diagram of the cuprates,[3,32] nor in other YBCO$_{6+x}$ samples at higher or lower doping levels (data not shown). Moreover, our measurements were taken in modest magnetic fields and on samples prepared in an identical fashion, which can be compared without any ambiguity. The quantitative disparity between diffraction and transport signatures of charge order is, therefore, an intrinsic feature of YBCO$_{6.67}$.

A possible solution to this conundrum is spatial inhomogeneity of the static charge order, which is indicated by the nonzero width of the diffraction features. X-ray scattering experiments with high energy resolution[49] indicate that the X-ray reflections originate predominantly from charge ordered domains nucleated by residual disorder—a finding that is also supported by NMR results[50]. If these domains are spatially disconnected, the current flow detected in transport experiments may predominantly originate from regions with weak or absent static charge order, thus explaining the quantitative disparity between the stress responses of static charge order and transport.

However, these considerations also show that static charge order is not responsible for the most prominent anomalous transport features of YBCO$_{6.67}$, including particularly the maximum and sign reversal of the Hall coefficient, which only depends weakly on stress (Fig. 4). In exploring alternative explanations, we can also rule out a Fermi-surface reconstruction by magnetic order, because static magnetism is not present in the YBCO system in the doping and magnetic-field range probed by our experiments. In principle, the unusual behavior of the Hall coefficient may arise from electronic correlations unrelated to density-wave order, including flux-flow phenomena in a phase-incoherent superconducting state that precedes superconducting long-range order. This scenario was invoked early on[51] to explain the sign reversal of R_H, but subsequent experiments have called this interpretation into question, based in part on the observed magnetic field independence of T_0, and on the continuous evolution of the low-field Hall coefficient into the quantum-oscillation regime that indicates a reconstructed Fermi surface in high magnetic fields[48]. Moreover, recent theoretical work indicates that phase-incoherent Cooper pairing does not reverse the sign of R_H[52]. Finally, we note that the superconducting transition temperature decreases (increases) under a-axis (b-axis) compression[45]. The stark contrast of this asymmetric strain response to the symmetric response of the normal-state resistivity and Hall effect is inconsistent with a major influence of superconductivity on the phenomena we have observed.

Conventional CDW order can thus be ruled out as the main origin of the transport anomalies, and one may ask whether slowly fluctuating, dynamical charge correlations recently uncovered by resonant inelastic X-ray scattering (RIXS)[3,53–56] offer an alternative explanation. These correlations grow strongly upon cooling, suggesting a critical divergence that is only cut off by the onset of superconductivity. Two factors argue in favor of such a scenario. First, the temperature evolution of the dynamical correlations is closely similar to that of the static order. Indeed, the diffraction features in elastic X-ray scattering can be understood as a 'central peak' resulting from pinning of low-energy collective charge fluctuations by defects[49]. The analogy between the T-evolution of charge order and transport coefficients pointed out above, therefore, also holds for dynamical correlations. Second, in contrast to the (slightly broadened) Bragg reflections manifesting static order, the dynamical charge correlations exhibit a ring-like pattern in reciprocal space[57], akin to analogous patterns in quantum spin liquids and superfluid helium. (Note that the ring pattern has thus far only been observed in Bi-based cuprates, but is also expected in YBCO$_{6.67}$ in view of the universality of the charge correlations in the cuprates[3].) Such liquid-like correlations (as well as the associated transport anomalies) are less directional in real space, and are hence expected to be less susceptible to stress along particular lattice directions than the static order. In a strongly fluctuating system, however, even a small stress-induced spectral-weight shift of the fluctuation spectrum may induce a
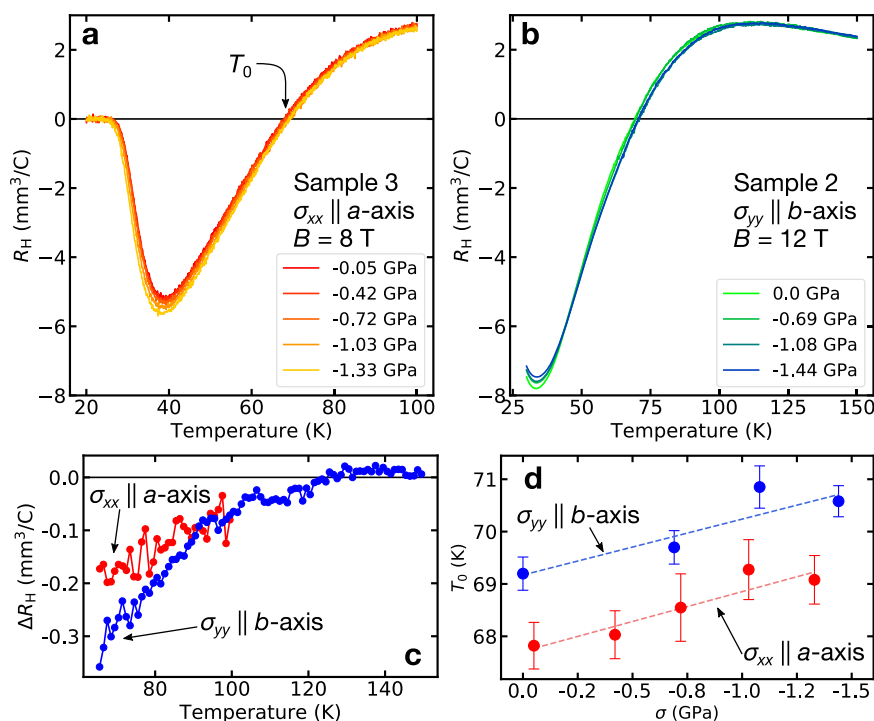
Fig. 4 Hall effect under uniaxial stress. Temperature dependence of the Hall coefficient in a magnetic field of 8 T under uniaxial stress along the a-axis (panel **a**) and in 12 T and along the b-axis (panel **b**). The stress amplitudes are shown in the legend. Note that the upturn of R_H upon cooling below ~40 K is due to the onset of superconductivity. **c** Difference between the Hall coefficients measured for $\sigma \sim -1$ GPa and $\sigma = 0$. **d** Sign reversal temperature T_0 as a function of stress. The error bars are the standard deviations of T_0.

large fractional response of the elastic 'tail' due to pinned fluctuations. This scenario can thus explain the quantitative disparity between the transport and diffraction features.

In summary, our investigation of the stress dependence of the resistivity and Hall coefficient of YBCO$_{6.67}$ has demonstrated surprising qualitative analogies to classical CDW materials with 2D electron systems, where the loss of scattering channels in the CDW state lowers the resistivity. Interestingly, the long-range-ordered 'striped' state in the La$_{2-x}$Ba$_x$CuO$_4$ family leads to an increase of the resistivity at the onset of charge order[58], possibly due to the influence of concomitant magnetic and lattice instabilities. In this context, we point out that the strain levels covered by our transport measurements were insufficient to reach the recently discovered state with 3D charge order in YBCO[29]. However, the momentum-integrated intensity of the X-ray diffraction features of 2D charge order largely exceeds the one of the 3D charge order (see Supplementary Note 5). Although these considerations suggest a dominant role of 2D charge order even at high strain levels, direct transport measurements in this regime are an interesting subject of future research.

Our data suggest a key role of liquid-like, nearly critical charge correlations for fermionic transport, in contrast to the electron–phonon-interaction driven static charge order in the classical systems. There have been a number of theoretical proposals along these lines, but few explicit calculations of transport coefficients. Calculations of the Hall coefficient in the framework of models with slowly fluctuating charge[36] or spin[59] order indicate a subtle downturn at low temperatures, but a sign reversal has not been predicted to the best of our knowledge. The concrete link between transport and scattering probes of charge correlations uncovered in our parametric study should motivate further progress in the development of this theoretical framework, for instance, by including the interplay with pairing fluctuations. On the experimental front, our study has demonstrated the power

of uniaxial-pressure experiments in the long-standing quest to establish correspondences between atomic-scale correlations and macroscopic transport in high-T_c superconductors. Extending this approach to other spectroscopic probes and other collective phenomena will open up new perspectives for quantum materials research.

METHODS

Transport measurements

Electrical contacts were prepared by sputtering Au on the surface[60]. Electrical resistivity (ρ) measurements were carried out along the stress direction by a standard ac lock-in method with a driving current of frequency ~80 Hz. Samples 1 and 3 (sample 2) thus yielded ρ_a (ρ_b) (Supplementary Note 6). Hall coefficient (R_H) measurements were carried out with magnetic field along the c-axis for samples 2 and 3. The measurements were performed with both positive and negative fields, to eliminate the contribution of the longitudinal magnetoresistivity.

DATA AVAILABILITY

Data that support the findings of this study are available from the corresponding authors upon reasonable request.

REFERENCES

1. Wu, T. et al. Emergence of charge order from the vortex state of a high-temperature superconductor. *Nat. Commun.* **4**, 2113 (2013).
2. Ghiringhelli, G. et al. Long-range incommensurate charge fluctuations in (Y,Nd) Ba$_2$Cu$_3$O$_{6+x}$. *Science* **337**, 821–825 (2012).

3. Frano, A., Blanco-Canosa, S., Keimer, B. & Birgeneau, R. J. Charge ordering in superconducting copper oxides. *J. Phys.: Condens. Matter* **32**, 374005 (2020).

4. Doiron-Leyraud, N. et al. Quantum oscillations and the Fermi surface in an underdoped high-T_c superconductor. *Nature* **447**, 565–568 (2007).

5. LeBoeuf, D. et al. Electron pockets in the Fermi surface of hole-doped high-T_c superconductors. *Nature* **450**, 533–536 (2007).

6. Proust, C. & Taillefer, L. The remarkable underlying ground states of cuprate superconductors. *Annu. Rev. Condens. Matter Phys.* **10**, 409–429 (2019).

7. Sebastian, S. E. et al. Metal-insulator quantum critical point beneath the high T_c superconducting dome. *Proc. Natl Acad. Sci. USA* **107**, 6175–6179 (2010).

8. Harrison, N. & Sebastian, S. E. Fermi surface reconstruction from bilayer charge ordering in the underdoped high temperature superconductor $YBa_2Cu_3O_{6+x}$. *N. J. Phys.* **14**, 095023 (2012).

9. Sebastian, S. E. & Proust, C. Quantum oscillations in hole-doped cuprates. *Annu. Rev. Condens. Matter Phys.* **6**, 411–430 (2015).

10. Chang, J. et al. Magnetic field controlled charge density wave coupling in underdoped $YBa_2Cu_3O_{6+x}$. *Nat. Commun.* **7**, 11494 (2016).

11. Gerber, S. et al. Three-dimensional charge density wave order in $YBa_2Cu_3O_{6.67}$ at high magnetic fields. *Science* **350**, 949–952 (2015).

12. Jang, H. et al. Coincident onset of charge-density-wave order at a quantum critical point in underdoped $YBa_2Cu_3O_x$. *Phys. Rev. B* **97**, 224513 (2018).

13. Lee, W.-S. X-ray studies of the CDW ground state and excitations in high-T_C cuprates. *J. Phys. Soc. Jpn.* **90**, 111004 (2021).

14. Souliou, S. M. et al. Rapid suppression of the charge density wave in $YBa_2Cu_3O_{6.6}$ under hydrostatic pressure. *Phys. Rev. B* **97**, 020503 (2018).

15. Putzke, C. et al. Charge order and superconductivity in underdoped $YBa_2Cu_3O_{7-\delta}$ under pressure. *Phys. Rev. Lett.* **120**, 117002 (2018).

16. Cyr-Choinière, O. et al. Sensitivity of T_c to pressure and magnetic field in the cuprate superconductor $YBa_2Cu_3O_y$: evidence of charge-order suppression by pressure. *Phys. Rev. B* **98**, 064513 (2018).

17. Vinograd, I. et al. Nuclear magnetic resonance study of charge density waves under hydrostatic pressure in $YBa_2Cu_3O_y$. *Phys. Rev. B* **100**, 094502 (2019).

18. Hicks, C. W. et al. Strong increase of T_c of Sr_2RuO_4 under both tensile and compressive strain. *Science* **344**, 283–285 (2014).

19. Steppke, A. et al. Strong peak in T_c of Sr_2RuO_4 under uniaxial pressure. *Science* **355**, eaaf9398 (2017).

20. Barber, M. E., Gibbs, A. S., Maeno, Y., Mackenzie, A. P. & Hicks, C. W. Resistivity in the vicinity of a van Hove singularity: Sr_2RuO_4 under uniaxial pressure. *Phys. Rev. Lett.* **120**, 076602 (2018).

21. Pfau, H. et al. Anisotropic quasiparticle coherence in nematic $BaFe_2As_2$ studied with strain-dependent ARPES. *Phys. Rev. B* **103**, 165136 (2021).

22. Grinenko, V. et al. Split superconducting and time-reversal symmetry-breaking transitions in Sr_2RuO_4 under stress. *Nat. Phys.* **17**, 748–754 (2021).

23. Li, Y. S., Borth, R., Hicks, C. W., Mackenzie, A. P. & Nicklas, M. Heat-capacity measurements under uniaxial pressure using a piezo-driven device. *Rev. Sci. Instrum.* **91**, 103903 (2020).

24. Ikeda, M. et al. Elastocaloric signature of nematic fluctuations. *Proc. Natl Acad. Sci. USA* **118**, e2105911118 (2021).

25. Watson, C. A., Gibbs, A. S., Mackenzie, A. P., Hicks, C. W. & Moler, K. A. Micron-scale measurements of low anisotropic strain response of local T_c in Sr_2RuO_4. *Phys. Rev. B* **98**, 094521 (2018).

26. Pustogow, A. et al. Constraints on the superconducting order parameter in Sr_2RuO_4 from oxygen-17 nuclear magnetic resonance. *Nature* **574**, 72–75 (2019).

27. Ghosh, S. et al. Piezoelectric-driven uniaxial pressure cell for muon spin relaxation and neutron scattering experiments. *Rev. Sci. Instrum.* **91**, 103902 (2020).

28. Qian, T. et al. Apparatus design for measuring of the strain dependence of the seebeck coefficient of single crystals. *Rev. Sci. Instrum.* **91**, 023902 (2020).

29. Kim, H.-H. et al. Uniaxial pressure control of competing orders in a high-temperature superconductor. *Science* **362**, 1040–1044 (2018).

30. Kim, H.-H. et al. Charge density waves in $YBa_2Cu_3O_{6.67}$ probed by resonant X-ray scattering under uniaxial compression. *Phys. Rev. Lett.* **126**, 037002 (2021).

31. Ishida, K. et al. Divergent nematic susceptibility near the pseudogap critical point in a cuprate superconductor. *J. Phys. Soc. Jpn.* **89**, 064707 (2020).

32. Blanco-Canosa, S. et al. Resonant X-ray scattering study of charge-density wave correlations in $YBa_2Cu_3O_{6+x}$. *Phys. Rev. B* **90**, 054513 (2014).

33. Harper, J. M. E., Geballe, T. H. & DiSalvo, F. J. Thermal properties of layered transition-metal dichalcogenides at charge-density-wave transitions. *Phys. Rev. B* **15**, 2943–2951 (1977).

34. Monceau, P. Electronic crystals: an experimental overview. *Adv. Phys.* **61**, 325–581 (2012).

35. Zhu, X., Guo, J., Zhang, J. & Plummer, E. W. Misconceptions associated with the origin of charge density waves. *Adv. Phys.: X* **2**, 622–640 (2017).

36. Caprara, S., Di Castro, C., Seibold, G. & Grilli, M. Dynamical charge density waves rule the phase diagram of cuprates. *Phys. Rev. B* **95**, 224511 (2017).

37. Lin, C. T., Zhou, W., Liang, W. Y., Schönherr, E. & Bender, H. Growth of large and untwinned single crystals of YBCO. *Physica C* **195**, 291–300 (1992).

38. Lindemer, T. B. et al. Experimental and thermodynamic study of non-stoichiometry in $YBa_2Cu_3O_{7-x}$. *J. Am. Ceram. Soc.* **72**, 1775–1788 (1989).

39. Lin, C. & Kulakov, A. In situ observation of ferroelastic detwinning of YBCO single crystals by high temperature optical microscopy. *Physica C* **408**, 27–29 (2004).

40. Liang, R., Bonn, D. A. & Hardy, W. N. Evaluation of CuO_2 plane hole doping in $YBa_2Cu_3O_{6+x}$ single crystals. *Phys. Rev. B* **73**, 180505 (2006).

41. Hicks, C. W., Barber, M. E., Edkins, S. D., Brodsky, D. O. & Mackenzie, A. P. Piezoelectric-based apparatus for strain tuning. *Rev. Sci. Instrum.* **85**, 065003 (2014).

42. Ando, Y., Komiya, S., Segawa, K., Ono, S. & Kurita, Y. Electronic phase diagram of high-T_c cuprate superconductors from a mapping of the in-plane resistivity curvature. *Phys. Rev. Lett.* **93**, 267001 (2004).

43. Barber, M. E., Steppke, A., Mackenzie, A. P. & Hicks, C. W. Piezoelectric-based uniaxial pressure cell with integrated force and displacement sensors. *Rev. Sci. Instrum.* **90**, 023904 (2019).

44. Barber, M. E. et al. Role of correlations in determining the Van Hove strain in Sr_2RuO_4. *Phys. Rev. B* **100**, 245139 (2019).

45. Barber, M. E. et al. Dependence of T_c of $YBa_2Cu_3O_{6.67}$ on in-plane uniaxial stress. *Phys. Rev. B* **106**, 184516 (2022).

46. Lei, M. et al. Elastic constants of a monocrystal of superconducting $YBa_2Cu_3O_{7-\delta}$. *Phys. Rev. B* **47**, 6154–6156 (1993).

47. Achkar, A. J. et al. Distinct charge orders in the planes and chains of ortho-III-ordered $YBa_2Cu_3O_{6+\delta}$ superconductors identified by resonant elastic X-ray scattering. *Phys. Rev. Lett.* **109**, 167001 (2012).

48. LeBoeuf, D. et al. Lifshitz critical point in the cuprate superconductor $YBa_2Cu_3O_y$ from high-field Hall effect measurements. *Phys. Rev. B* **83**, 054506 (2011).

49. Le Tacon, M. et al. Inelastic X-ray scattering in $YBa_2Cu_3O_{6.6}$ reveals giant phonon anomalies and elastic central peak due to charge-density-wave formation. *Nat. Phys.* **10**, 52–58 (2014).

50. Wu, T. et al. Incipient charge order observed by NMR in the normal state of $YBa_2Cu_3O_y$. *Nat. Commun.* **6**, 6438 (2015).

51. Harris, J. M. et al. Additive quasiparticle and vortex Hall conductivities in $La_{2-x}Sr_xCuO_4$ and untwinned $YBa_2Cu_3O_{6.93}$. *Phys. Rev. B* **51**, 12053–12056 (1995).

52. Boyack, R., Wang, X., Chen, Q. & Levin, K. Combined effects of pairing fluctuations and a pseudogap in the cuprate Hall coefficient. *Phys. Rev. B* **99**, 134504 (2019).

53. da Silva Neto, E. H. et al. Coupling between dynamic magnetic and charge-order correlations in the cuprate superconductor $Nd_{2-x}Ce_xCuO_4$. *Phys. Rev. B* **98**, 161114 (2018).

54. Miao, H. et al. Formation of incommensurate charge density waves in cuprates. *Phys. Rev. X* **9**, 031042 (2019).

55. Yu, B. et al. Unusual dynamic charge correlations in simple-tetragonal $HgBa_2CuO_{4+\delta}$. *Phys. Rev. X* **10**, 021059 (2020).

56. Huang, H. Y. et al. Quantum fluctuations of charge order induce phonon softening in a superconducting cuprate. *Phys. Rev. X* **11**, 041038 (2021).

57. Boschini, F. et al. Dynamic electron correlations with charge order wavelength along all directions in the copper oxide plane. *Nat. Commun.* **12**, 597 (2021).

58. Li, Q., Hücker, M., Gu, G. D., Tsvelik, A. M. & Tranquada, J. M. Two-dimensional superconducting fluctuations in stripe-ordered $La_{1.875}Ba_{0.125}CuO_4$. *Phys. Rev. Lett.* **99**, 067001 (2007).

59. Storey, J. G. Hall effect and Fermi surface reconstruction via electron pockets in the high-T_c cuprates. *Europhys. Lett.* **113**, 27003 (2016).

60. Ekin, J. W. et al. High T_c superconductor/noble-metal contacts with surface resistivities in the 10^{-10} Ωcm^2 range. *Appl. Phys. Lett.* **52**, 1819–1821 (1988).

61. Momma, K. & Izumi, F. *VESTA3* for three-dimensional visualization of crystal, volumetric and morphology data. *J. Appl. Crystallogr.* **44**, 1272–1276 (2011).

ACKNOWLEDGEMENTS

AUTHOR CONTRIBUTIONS

S.N., P.Y., M.E.B., and K.I. performed the transport measurements. S.N. analyzed the data. S.N., H.-H.K., and T.L. prepared the single crystals studied in the present work. The uniaxial stress devices were built by P.Y., M.E.B., and C.W.H. B.K., M.L.T., M.M., C.W.H., and A.P.M. supervised the project. S.N., M.M., and B.K. wrote the manuscript with suggestions from all coauthors.

FUNDING

COMPETING INTERESTS

The authors declare no competing interests.

ADDITIONAL INFORMATION

Supplementary information The online version contains supplementary material available at https://doi.org/10.1038/s41535-022-00532-9.

Correspondence and requests for materials should be addressed to B. Keimer.

Reprints and permission information is available at http://www.nature.com/reprints

Publisher's note Springer Nature remains neutral with regard to jurisdictional claims in published maps and institutional affiliations.